Electromagnetic Interference Pattern of Resonance Cones in the Far Field

Paul M. Bellan
California Institute of Technology, Pasadena, California 91125
(Received 26 December 1979)

At large densities or large distances from the transmitting antenna it is observed that resonance cones, instead of being a single sharp peak, become spatially modulated by a multiperiod interference pattern; this interference pattern can dominate over the phasing imposed by a grill antenna. A simple theory shows that this effect occurs when $\omega_{pe} r/c \gg 1$ and that it is caused by electromagnetic terms neglected in the electrostatic approximation.

PACS numbers: 52.40.Db, 52.35.Fp, 52.50.Gj, 52.40.Fd

Lower-hybrid waves, a potentially attractive means for heating plasmas to fusion ignition,[1] have been thoroughly studied in several small-scale nontokamak experiments[2-5] and the wave propagation observed was consistent with electrostatic theory.

The propagation of both grill[6] and probe excited waves has been examined in the Caltech Encore tokamak (major radius 38 cm, minor radius 12 cm). Because Encore has an extremely high repetition rate (10–30 shots/sec) and also modest plasma parameters ($n \sim 10^{12}$ cm^{-3}, toroidal $B \sim 0.5$–1.6 kG, $I_p \sim 0.6$–6 kA, $T_e \sim 10$ eV, shot duration ~ 2 msec, Ar gas) detailed interferometric probe measurements of the wave propagation are possible. These measurements, which I present here, demonstrate that the antenna excites a complex interference pattern rather than the "image" of itself predicted by electrostatic theory. I also present an analysis (with corroborating probe measurements) showing that electromagnetic terms (neglected in electrostatic theory) cause this interference pattern. These electromagnetic terms become important when $\omega_{pe} r/c \gg 1$, where r is the distance from the antenna. The nonobservance of the electromagnetic interference pattern in Refs. 2–5 is consistent with these experiments having $\omega_{pe} r/c \ll 1$. Like Encore, large tokamaks (e.g., Alcator, Princeton Large Torus, etc.) have $\omega_{pe} r/c \gg 1$; thus the electromagnetic interference effect should occur in these devices as well. In Encore this interference pattern dominated the grill-imposed phasing at large r; the same effect can be expected in the large tokamaks.

Figure 1(a) shows the Encore experimental setup. Linear waves ($\omega/2\pi \sim 300$–800 MHz, $P \ll 1$ W) are excited by a four-port "grill" ($\lambda_z = 3.5$ cm, 16 cm high) or by a probe. The waves in the plasma are picked up by probes which traverse the minor radius [top and side probes, Fig. 1(a)] or which make a circle [dashed line, Fig. 1(a)] in the device midplane. The probe signal goes to an rf interferometer, the output of which is sampled during each plasma shot and averaged over several shots by a boxcar integrator.

Figure 1(b), a circle probe interferogram, shows that, when the plasma is off, the grill antenna generates the expected two-period vacuum field pattern, but when the plasma is on, the probe additionally picks up both the parallel and antiparallel (to $\vec{B}$) resonance cones, each two periods long. Thus, near the antenna the wave follows electrostatic resonance-cone theory.[2,3,5]

Figure 2(a) shows radial interferograms made with a side probe located a toroidal angle of 108° from the grill. Instead of the two wavelengths predicted by electrostatic theory, there now is a multiperiod interference pattern. The envelope of the interference pattern follows the resonance-cone angle, θ_c, since for decreasing B the interference envelope moves to the left, i.e., larger θ_c ($\theta_c \simeq \omega/\omega_{ce}$ since $\omega_{pe} \gg \omega_{ce}$ for Encore).

Figure 2(b) shows that each grill port excites this complicated interference pattern. The port-to-port radial shift of the fringes [cf. dashed line, Fig. 2(b)] shows that the interference pattern follows the resonance cone trajectory. The overall radial shift from the top to the bottom traces of

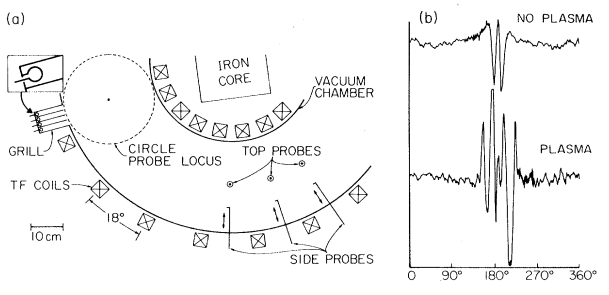

FIG. 1. (a) Encore setup, grill ports are loop-coupled (inset). (b) Grill excitation, circle probe interferogram, $f = 700$ MHz, $B = 1.6$ kG.

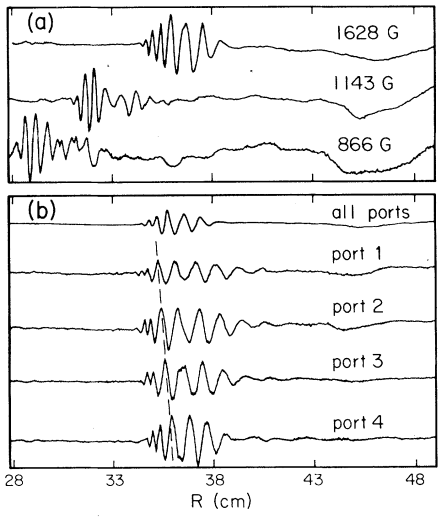

FIG. 2. Grill excitation, $f = 650$ MHz, side probe (108° toroidal separation from grill) interferograms. (a) Variation of B. (b) Variation of connection to grill ports, $B = 1.6$ kG, dashed line shows constant phase surface.

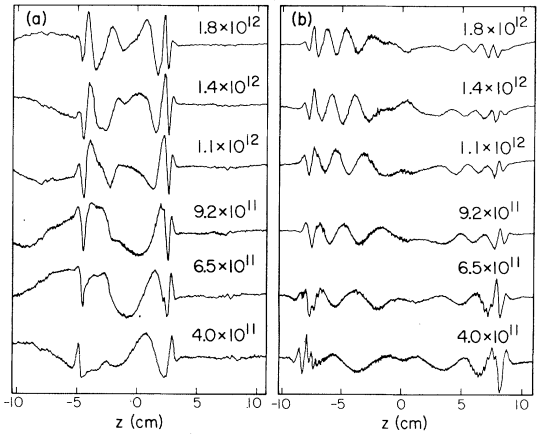

FIG. 3. Probe excitation (probe at plasma center), receiving probe moves vertically, $f = 650$ MHz, $B = 0.7$ kG, density varied. (a) Toroidal separation = 18°, i.e., $r = 12$ cm; (b) toroidal separation 36°, $r = 24$ cm.

Fig. 2(b) is $\Delta r/\Delta z \simeq 0.14$, in reasonable agreement with $\theta_c \simeq \omega/\omega_{ce} = 0.15$. Thus, the interference pattern phase fronts parallel the resonance cone asymptotes.

This agreement with simple electrostatic theory in the near field, but degeneration into an interference pattern in the far field, has also been observed when probe transmitting antennas were used. Because probes generate a simpler, more symmetric signal than the grill, they provide a clearer picture of what is happening. To further simplify the interpretation of the interference pattern, the transmitting probe was located at the center of the minor cross section and the receiving probe scanned vertically, so that the cone was vertically symmetrical (since $\partial B/\partial z = 0$).

Figures 3(a) and 3(b) show interferograms for sequences of plasma densities[7] with the transmitting and receiving probes toroidally separated by 18° and 36°, respectively. At low densities and small separations [bottom of Fig. 3(a)] the trace resembles the electrostatic resonance cone. With increasing density, additional interference fringes come into existence; however, θ_c does not change. Figure 3(b) shows the same behavior except (i) left and right patterns are further separated (in agreement with $\theta_c \simeq \omega/\omega_{ce} = 0.33$), (ii) each pattern has more fringes, and (iii) a shorter-wavelength interference pattern is also visible in the bottom two traces.

These experimental results show that near the antenna (grill or probe) the field agrees with electrostatic cone theory, but far from the antenna and at higher densities the cone becomes the asymptote of a multifringe interference pattern which, in the case of the grill, dominates the phasing imposed on the grill. Furthermore, there is a second interference pattern [cf. bottom of Fig. 3(b)] having shorter wavelengths. A typical density profile for the data of Fig. 3 is shown in Fig. 4(a); Fig. 4(b) shows that the fringe envelope moves as a resonance cone when the frequency is varied.

I now show that (i) the dominant interference pattern comes from electromagnetic terms neglected in the electrostatic theory, and (ii) the shorter-wavelength interference pattern is the well-known[2,4,8] thermal interference pattern.

The cold slow wave dispersion (for $D, |P| \gg S$) can be written as

$$n_\perp^2 = (-P/2S)\{n_z^2 - (S - D^2/P) + [(n_z^2 - n_{\rm acc}^2)(n_z^2 - n_b^2)]^{1/2}\}, \quad (1)$$

where $\vec{n} = c\vec{k}/\omega$ is the refractive index, $S = 1 - \omega_{pi}^2/\omega^2 + \omega_{pe}^2/\omega_{ce}^2$, $P = 1 - \omega_{pe}^2/\omega^2$, $D = \omega_{pe}^2/\omega\omega_{ce}$, $n_{\rm acc} = S^{1/2} + (-D^2/P)^{1/2}$ is the minimum n_z for constant-density accessibility, and $n_b = S^{1/2} - (-D^2/P)^{1/2}$. If n_z^2

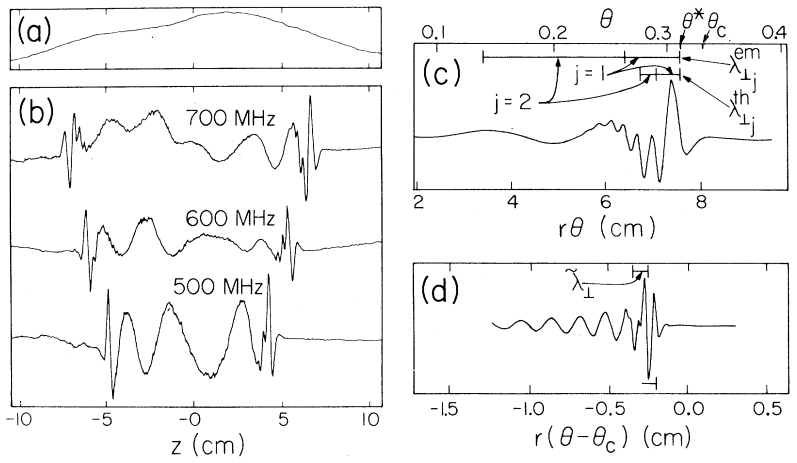

FIG. 4. (a) Typical density profile; (b) variation of frequency, probe excitation, $B=0.87$ kG; (c) numerical integration of Eq. (4) for Encore [cf. Fig. 3(b)] $f=650$ MHz, $r=24$ cm, $B=0.7$ kG, $n=6.5\times10^{11}$, $T=10$ eV, Ar; (d) numerical integration of Eq. (4) for Alcator (Ref. 9): $f=2.5$ GHz, $r=85$ cm, $B=60$ kG, $T=1$ keV, $n=2\times10^{14}$, D.

$\gg n_{acc}{}^2$, then Eq. (1) becomes

$$n_\perp{}^2=(-P/S)[n_z{}^2-(S-D^2/P)]. \quad (2)$$

In the electrostatic approximation $S-D^2/P$ is dropped from Eq. (2), making $k_\perp$ proportional to k_z, directly giving resonance cones.

If $S-D^2/P$ (i.e., the lowest-order electromagnetic correction) is retained, and thermal corrections[8] and Landau damping[8] are included, the dispersion $\vec{\kappa}=\vec{k}r$ is

$$\kappa_\perp=\kappa_z{}^{-1}(\omega_{pe}r/c)^2\mu\tan\theta_c-\kappa_z\cot\theta_c-\kappa_z{}^3\alpha(r_L/r)^2+i\delta\kappa_z, \quad (3)$$

where $\mu=\frac{1}{2}(S-D^2/P)/S$, $\theta_c=\tan^{-1}|S/P|^{1/2}$, r_L is the electron Larmor radius, and α (thermal coefficient), δ (Landau damping) are defined by Eq. (20) of Ref. 8. For $\omega^2\gg\omega_{lh}{}^2$ (e.g., Encore), $\mu\simeq\frac{1}{2}(1+2\omega_{pe}{}^2/\omega_{ce}{}^2)/(1+\omega_{pe}{}^2/\omega_{ce}{}^2)$, and so $\frac{1}{2}<\mu<1$. The respective terms in Eq. (3) are electromagnetic correction, cold resonance cone, thermal correction, and Landau damping.

Extending Kuehl's formalism,[8] the potential excited by a point source is

$$\Phi(\vec{r})\sim\int_{\omega r n_{acc}/c}^{\infty}\frac{d\kappa_z\exp[if(\kappa_z)]}{Sr[\kappa_\perp(\kappa_z)\sin\theta]^{1/2}}, \quad (4)$$

where $\theta=\cos^{-1}(\hat{\vec{r}}\cdot\hat{\vec{B}})$, $f(\kappa_z)=\kappa_z\cos\theta+\kappa_\perp\sin\theta$. If Eq. (2) holds (i.e., $\kappa_z\gg\omega r n_{acc}/c$) then $f\simeq a/\kappa_z+b\kappa_z-d\kappa_z{}^3+i\gamma(\kappa_z)$, where $a=(\omega_{pe}r/c)^2\mu\sin\theta\tan\theta_c$, $b=\sin(\theta_c-\theta)/\sin\theta_c$, $d=\alpha(r_L/r)^2\sin\theta$, and $\gamma(\kappa_z)=\kappa_z\delta\sin\theta$. Since *electromagnetic effects are now included* (finite a) the phase in the Eq. (4) integrand has *two* saddle points [i.e., $f'(\kappa_z)=0$] at $\kappa_z{}^2=[b\pm(b^2-12ad)^{1/2}]/6d$. These coalesce when $b^2=12ad$ which occurs at $\theta^*=\theta_c-\sin^{-1}[2(\omega_{pe}r_L/c)\sin^2\theta_c\times(3\mu\alpha\tan\theta_c)^{1/2}]$; the coalesced κ_z is $\kappa_z{}^*\equiv(a/3d)^{1/4}$. For $b^2\gg12ad$ the respective thermal[2,4,8] and *electromagnetic* saddle points are at $\kappa_z{}^{th}=(b/3d)^{1/2}$ and $\kappa_z{}^{em}=(a/b)^{1/2}$. This saddle-point analysis breaks down when $\kappa_z{}^{em}\to\omega r n_{acc}/c$ since Eq. (2) then becomes invalid; this occurs for $\theta\ll\theta_c$, i.e., $b\to1$. When $b^2\gg12ad$, steepest-descent integration of Eq. (4) gives

$$\Phi(r)\sim\frac{\pi^{1/2}\sin\theta_c\{\exp[i\xi_{th}-\gamma(\kappa_z{}^{th})]+i\exp[i\xi_{em}-\gamma(\kappa_z{}^{em})]\}}{Sr[-i\sin(\theta_c-\theta)\sin\theta\cos\theta_c]^{1/2}}, \quad (5)$$

where $\xi_{th}=2(b/3)^{3/2}d^{-1/2}$ and $\xi_{em}=2(ab)^{1/2}$ are the phases of the respective thermal and electromagnetic terms. The location of the j^{th} fringe, θ_j, is determined by $\xi-f(\kappa_z{}^*)=2j\pi$, where $\xi=\xi_{em}$ or ξ_{th} for electromagnetic or thermal fringes and ξ depends on θ_j through b. Here $f(\kappa_z{}^*)[=8(da^3/27)^{1/4}]$ is the phase at θ^*. Hence $\theta_j{}^{th}=\theta_c-\sin^{-1}\{3\times d^{1/3}\sin\theta_c[j\pi+f(\kappa_z{}^*)/2]^{2/3}\}$, while $\theta_j{}^{em}=\theta_c-\sin^{-1}\{a^{-1}\sin\theta_c[j\pi+f(\kappa_z{}^*)/2]^2\}$. The first fringe has width $\Delta\theta_1=\theta_1-\theta^*$, while subsequent ($j\geq1$) fringes have widths $\Delta\theta_{j+1}=\theta_{j+1}-\theta_j$; corresponding radial wavelengths are $\lambda_{\perp j}=r\Delta\theta_j$.

Typical Encore parameters [e.g., second from bottom trace, Fig. 3(b)] of $\theta_c\simeq\omega/\omega_{ce}\simeq0.33$, $r_L=10^{-2}$ cm, $r=24$ cm, $\omega_{pe}r/c\simeq35$, $\mu\simeq1$, $\alpha\simeq\frac{11}{8}(\omega_{ce}/$

$\omega)^3$ [since $\omega_{pe} \gg \omega_{ce}$, $\omega \ll \omega_{ce}$], give $\theta^* \simeq 0.31$, $\lambda_{\perp_1}^{em} = 1.5$ cm, $\lambda_{\perp_2}^{em} = 2.7$ cm and $\lambda_{\perp_1}^{th} = 0.5$ cm, $\lambda_{\perp_2}^{th} = 0.3$ cm, in good agreement with the experimental observations. For larger j the thermal fringes become shorter and are strongly Landau damped, while the electromagnetic fringes get longer. Also for larger j the electromagnetic saddle-point solution becomes invalid because κ_z^{em} becomes smaller than $\omega r n_{acc}/c$. To determine what happens when this occurs, Eq. (4) has been integrated numerically using Eq. (1) (with thermal corrections and Landau damping added) for $\kappa_\perp$. Figure 4(c) shows the results of such an integration for the above Encore parameters; for comparison θ_c, θ^*, and the $\lambda_\perp$'s calculated above are also shown.

Extrapolating this analysis to the parameters of a typical large tokamak, say Alcator[9] ($f = 2.5$ GHz, $B = 60$ kG, $T_e = 1$ keV, density $= 2\times10^{14}$), and using $r = 85$ cm (corresponding to 90° around the 54-cm-major-radius torus), gives $\theta_c = 2\times10^{-2}$, $\omega_{pe} r/c = 2\times10^3$, $\mu = 0.8$, $\alpha = 3\times10^5$ (finite T_1 causes negligible modification of Kuehl's α), and $r_L = 1.3\times10^{-3}$ cm, so that $\theta^* = 1.7\times10^{-2}$ and $\lambda_{\perp_1}^{em} = 0.1$ cm, $\lambda_{\perp_2}^{em} = 0.14$ cm, while $\lambda_{\perp_1}^{th} = 0.1$ cm, $\lambda_{\perp_2}^{th} = 0.04$ cm. These λ's are comparable to the expected grill imposed $\lambda_\perp$. Figure 4(d) shows the numerically integrated Eq. (4) for these parameters; numerical integration limits correspond to an accessibility window of $1.7 < n_z < 6$ [lower limit from n_{acc}, upper from $\gamma(\kappa_z) > 5$]. For comparison Fig. 4(d) also shows $\tilde{\lambda}_\perp$, the $\lambda_\perp$ corresponding to $n_z = 3$, the dominant Alcator grill n_z (coalescence of the electromagnetic and thermal saddle points is also at $n_z \simeq 3$).

In conclusion, this interference effect comes from a "dispersion" (i.e., deviation from linearity) in the dependence of k_x on k_z; the source k_z spectrum is *not* modified (as might first seem). Hence this effect will not alter a particular antenna's accessibility or heating properties (to the extent that the latter depend only on k_z, as in Landau damping). The effect occurs when the source k_z spectrum is broad enough to generate a range of interfering k_x's—i.e., a source perfectly monochromatic in k_z would not have an interference pattern. Typical (i.e., 2–4 port) grill antennas *do* have a broad k_z spectra and so, at large $\omega_{pe} r/c$, should exhibit the electromagnetic interference pattern.

The author wishes to thank E. Fredrickson for help in constructing the probes, and H. M. Simpson and F. T. Cosso for help in constructing Encore. This work has been supported by National Science Foundation Grant No. ENG78-05784, by the Ford-Exxon Energy Fund, by the California Insititute of Technology Institutional Energy Program, and by U. S. Department of Energy Contract No. EY-76-G-03-1305. The author is an Alfred P. Sloan Fellow.

[1]W. M. Hooke, in Proceedings of the Third Topical Conference on RF Plasma Heating, Pasadena, 1978 (unpublished), Paper No. A2, and references therein.

[2]R. K. Fisher and R. W. Gould, Phys. Fluids 14, 857 (1971).

[3]R. J. Briggs and R. R. Parker, Phys. Rev. Lett. 29, 852 (1972).

[4]A. Gonfalone, J. Phys. (Paris) 33, 521 (1972).

[5]P. Bellan and M. Porkolab, Phys. Rev. Lett. 34, 124 (1975).

[6]M. Brambilla, Nucl. Fusion 16, 47 (1976).

[7]Measured with a Langmuir probe, with use of the calibration factor of J. G. Laframboise, University of Toronto, Institute of Aerospace Studies Report No. 100, 1966 (unpublished).

[8]H. H. Kuehl, Phys. Fluids 16, 1311 (1973).

[9]J. J. Schuss *et al.*, Phys. Rev. Lett. 43, 274 (1979); see also C. M. Surko *et al.*, Phys. Rev. Lett. 43, 1016 (1979).